Single-Molecule Electrical Currents Associated with

Valinomycin Transport of K<sup>+</sup>

Alexandra J. Schmeltzer, Joel M. Harris\*, and Henry S. White\*

Department of Chemistry, University of Utah; Salt Lake City, UT 84112, USA

\*Correspondence to: harrisi@chem.utah.edu, white@chem.utah.edu

ABSTRACT: A quantitative description of ionophore-mediated ion transport is important in

understanding ionophore activity in biological systems and developing ionophore applications.

Herein, we describe the direct measurement of the electrical current resulting from K<sup>+</sup> transport

mediated by *individual* valinomycin (val) ionophores. Step fluctuations in current measured across

a 1,2-diphytanoyl-sn-glycero-3-phosphocholine (DPhPC) bilayer suspended over a ~400 nm

radius glass nanopore result from dynamic partitioning of val between the bilayer and torus region,

effectively increasing or decreasing the total number of val present in the membrane. In our studies,

approximately 30 val are present in the membrane on average with a val entering or leaving the

bilayer approximately every 50 seconds, allowing measurement of changes in electrical current

associated with individual val. The single-molecule val(K<sup>+</sup>) transport current at 0.1 V applied

potential is  $(1.3 \pm 0.6) \times 10^{-15}$  A, consistent with estimates of the transport kinetics based on large

val ensembles. This methodology for analyzing single ionophore transport is general and can be

applied to other carrier-type ionophores.

KEYWORDS: single-molecule, valinomycin, ionophore, femptoampere, electron shot noise,

nanopore

1

Valinomycin (*val*) is a well-known K<sup>+</sup> transporter,<sup>1-3</sup> and an effective antibiotic agent.<sup>4-6</sup>

Val was isolated by Brockmann and Schmidt-Kastner in 1955,<sup>7</sup> and later identified as an antibiotic against *Mycobacterium tuberculosis*.<sup>8</sup> Additional applications of *val* include its use in studies of K<sup>+</sup> uptake by cellular mitochondria,<sup>1,2</sup> and probing the bacterial phosphorylation mechanism.<sup>9</sup> Val has been widely used for decades as a model in studying ion-carrier transport across bilayers and in preparation of K<sup>+</sup> ion-selective membranes.<sup>10,11</sup> Recent investigations of *val* as a potent antiviral agent against coronaviruses have been reviewed.<sup>6,12</sup>

*Val* is well-established as a carrier-type ionophore.<sup>13-31</sup> It comprises a 12-membered cyclodepsipeptide with a hydrophobic exterior and hydrophilic interior (Figure 1), enabling the binding and transport of alkali metal cations across lipid membranes.<sup>8, 13, 15, 31</sup> *Val* is one example of many carrier-type ionophores (*e.g.*, monensin, nigericin, and enniatin B)<sup>19, 27</sup> capable of transporting individual ions across lipid bilayer structures including cell membranes.<sup>25, 26</sup> The unidirectional bilayer transport of K<sup>+</sup> by *val* across bilayers under the influence of an applied voltage results in a measured electrical current,<sup>21, 32, 33</sup> similar to membrane ion channels such as α-hemolysin<sup>34, 35</sup> and gramicidin.<sup>17, 36</sup> However, unlike ion channels, which span the bilayer and transport ions sufficiently fast to allow single-channel electrical characterization, ion-carriers bind and transport one ion at a time across the bilayer.<sup>16, 18, 22, 24, 35</sup> Ion channels transport multiple ions at once, whereas ion-carriers only transport one ion at a time.<sup>22</sup> Characterizing the ion transport properties of carrier-type ionophores is challenging due to the low rate of ion transport, resulting in low electrical currents.<sup>18</sup> Reports to date of carrier-type ionophore kinetics rely on ensemble measurements of ion transport rather than single-molecule studies.<sup>13, 14, 23, 30-32, 37</sup>

One such ensemble-type analysis of a carrier ionophore, performed by Stark and coworkers, detailed the effects of temperature, cation species, and phospholipid chain length on

val faciliated K+ transport across bilayers, resulting in the transport model shown in Figure 1.  $^{14, 23, 30, 37}$  Steady state and pulsed current measurements revealed four steps associated with one val transport cycle: (i) K<sup>+</sup> binding to val to form the val(K<sup>+</sup>) complex; (ii) transport of val(K<sup>+</sup>) under the influence of an electric field ( $\sim 10^5$  V/cm); (iii) release of K<sup>+</sup>; and (iv) diffusion of val back across the bilayer. The binding of K<sup>+</sup> to val (step (i)) and transport of the ion (ii) were found to be dependent on  $V_{\rm app}$ , as described by the expression  $k = k^0 \exp(V_{\rm app}F/2RT)$ , where  $k^0$  is the binding or transport rate under zero applied bias, F is Faraday's constant, R is the gas constant, and T is the temperature.  $^{30}$  In a 0.5 M KCl solution, the rate of val(K<sup>+</sup>) unbinding (step (iii)) and the diffusion of the un-complexed val back across the membrane (step (iv)) were reported to be the rate-limiting steps.  $^{14}$ 

The characteristic time,  $\tau$ , required for one *val* molecule to transport individual K<sup>+</sup> across the membrane is estimated from the first-order rate constants of the rate-limiting steps (*i.e.*,  $val(K^+)$  unbinding and the diffusion of the un-complexed val),

$$\tau = (2.4 \times 10^4 \text{ s}^{-1})^{-1} + (1.5 \times 10^4 \text{ s}^{-1})^{-1}$$
 (1)

yielding,  $\tau = 1.1 \times 10^{-4}$  s. Thus, on average, one *val* transports  $\sim 10^4$  K<sup>+</sup> across the bilayer per second, corresponding to an electrical current on the order of  $\Delta i \approx 1.5 \times 10^{-15}$  A (1.5 fA), where  $\Delta i$  is the fundamental descriptor of ionophore transport efficiency.

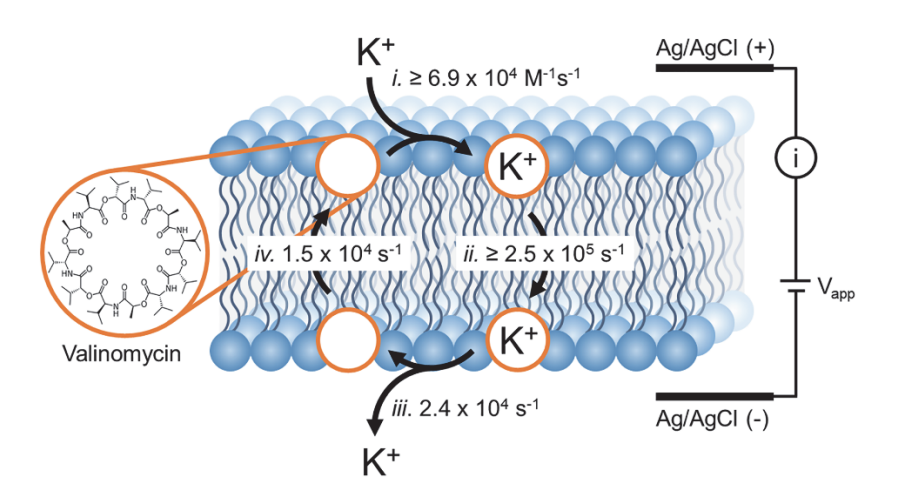


Figure 1. The transport model and rate constants of val-mediated K<sup>+</sup> transport across a lipid bilayer. Val = 0. The rates of steps (i) and (ii) were calculated using  $k = k^0 \exp(V_{app}F/2RT)$  with  $k^0$  values reported in ref. 37 and  $V_{app} = 0.1$  V (see Table S1). Bias-independent rate constants for steps (iii) and (iv) are reported in ref. 37. Figure is not drawn to scale.

For comparison, ionic currents associated with membrane ion channels (*e.g.* gramicidin<sup>2,36</sup> and  $\alpha$ -hemolysin)<sup>34,35</sup> are 10<sup>2</sup> to 10<sup>4</sup> times larger (100 fA–10 pA), and are readily quantified. However, the small current estimated for *val* carrier transport approaches the shot noise limit of electrical current measurements, theoretically equal to  $\pm 100~e^-/\Delta t$  (in the absence of a baseline current), where  $\Delta t$  is the time over which the current is measured.<sup>38</sup> Thus, a  $\Delta t = 1$  s measurement of the anticipated current due to *val* transport of K<sup>+</sup> (1.5 fA) corresponds to ~10,000  $e^-$ , well above the theoretical limit of quantification.<sup>38</sup>

Herein, we report measurements of the electrical current resulting from individual val transport of  $K^+$  across a DPhPC bilayer membrane. Low noise-level current measurements are achieved through the use of highly stable bilayers (18 hr lifetime, Figures S1–S2) suspended across a ~400 nm radius orifice of a conical nanopore in a glass membrane, Figure 2.<sup>35, 39</sup> Our strategy to measure the current associated with an individual val is based on the small area of the bilayer

( $\sim$ 5×10<sup>-9</sup> cm<sup>2</sup>), which limits the number of *val* within the active transport area, thus providing a means to conduct electrical measurements on a small population of *val* ( $\sim$ 30 molecules). Dynamic partitioning of *val* between the bilayer and the torus region containing excess lipid and solvent (decane) allows observation of step changes in electrical current associated with an individual *val*. <sup>14, 40</sup>

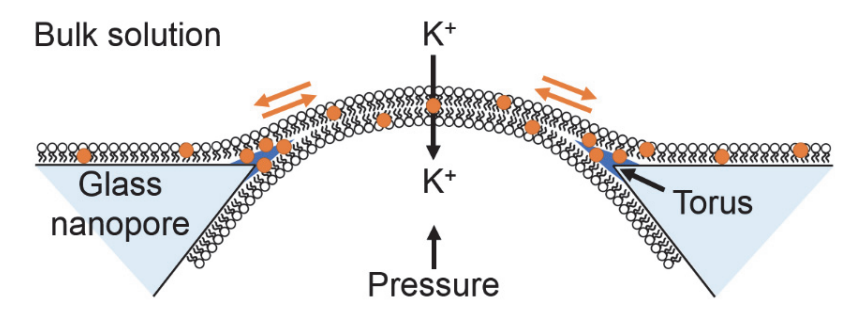


Figure 2. Schematic of a lipid bilayer formed over a glass nanopore support with val ( $\bullet$ ) present in the lipid phase. An applied voltage drives K<sup>+</sup> transport across the bilayer (see Figure 1). A pressure of 20 mmHg is applied from the interior of the nanopore to join the two lipid leaflets.<sup>41</sup> The torus region at the circumference of the membrane contains excess lipid, solvent, and val.<sup>40</sup> Val partitions between the bilayer area and the torus region changing the number of val within the bilayer. The electrical current is proportional to the number of val in the bilayer at any instant.<sup>14</sup> Figure is not drawn to scale.

# RESULTS AND DISCUSSION

Spontaneous Val Membrane Insertion and Ion Transport Selectivity. Lipid bilayers suspended across the nanopore orifice (Figure 2) were prepared by depositing a lipid solution consisting of **DPhPC** 3lipid and decane nanopore silanized with onto glass cyanopropyldimetyhlchlorosilane.<sup>35</sup> To form the bilayer, a 0.05 µL aliquot of the lipid solution was gently placed on top of the electrolyte solution exterior to the nanopore. The electrolyte solution level was then raised and lowered with respect to the nanopore to deposit two suspended lipid leaflets, separated by decane, across the nanopore orifice. A pressure of 20 mmHg was

applied and maintained inside the nanopore to join the leaflets, forming a bilayer.<sup>35</sup> A 0.1 V bias was applied across the membrane using two Ag/AgCl electrodes (one inside the nanopore and one external in the bulk solution), and the *i-t* trace recorded for ~2 hours to establish a baseline current in the buffered electrolyte (in the absence of *val*). Bilayer baseline currents measured using glass nanopores were stable for extended periods of time (18 hr, Figure S1). All data were recorded at a 5 kHz acquisition rate using a 1 kHz low-pass filter (LPF). Post data collection, data were resampled at 2 Hz and filtered with a 1 Hz LPF. The electrical noise of the measurement post-filtering was on the order of 1 fA. The *i-t* traces are intentionally presented without correction for the instrumental baseline current, which is significant and difficult to offset when working at fA current levels. As discussed below, baseline currents influence the limit of quantification of currents associated with individual *val*.

Prior to measurements of the K<sup>+</sup> current associated with a single val, we first established that our nanopore/bilayer system yielded results in agreement with literature data detailing  $val(K^+)$  transport across 0.1–3 mm diameter bilayer membranes.<sup>14</sup> Figure 3 shows experimental i-t traces recorded in buffered electrolyte solutions containing 0.5 M RbCl, KCl, or NaCl, prior to and following the addition of val to the electrolyte. In agreement with prior reports, val spontaneously inserts into the membrane when introduced at a concentration of  $10^{-6}$  to  $10^{-7}$  M to the exterior electrolyte solution at  $V_{app} = 0.1$  V, as indicated by an immediate increase in current across the bilayer (Figure S3, Table S2).<sup>14, 42, 43</sup> The increase in current shown in Figure 3A, B, and C result from val facilitating transport of Rb<sup>+</sup>, K<sup>+</sup>, or Na<sup>+</sup> across the membrane. After ~2 hr, the electrical current approaches an apparent steady state value,  $i_{ss}$ , that is dependent upon the cation species and the initial concentration of val. As Figure 3 indicates, we find that  $i_{ss}(Rb^+) > i_{ss}(K^+) >> i_{ss}(Na^+)$ , in

agreement with prior reports.<sup>44, 45</sup> No increase in current was observed when *val* was introduced into a solution containing 0.1 M KClO<sub>4</sub> electrolyte.

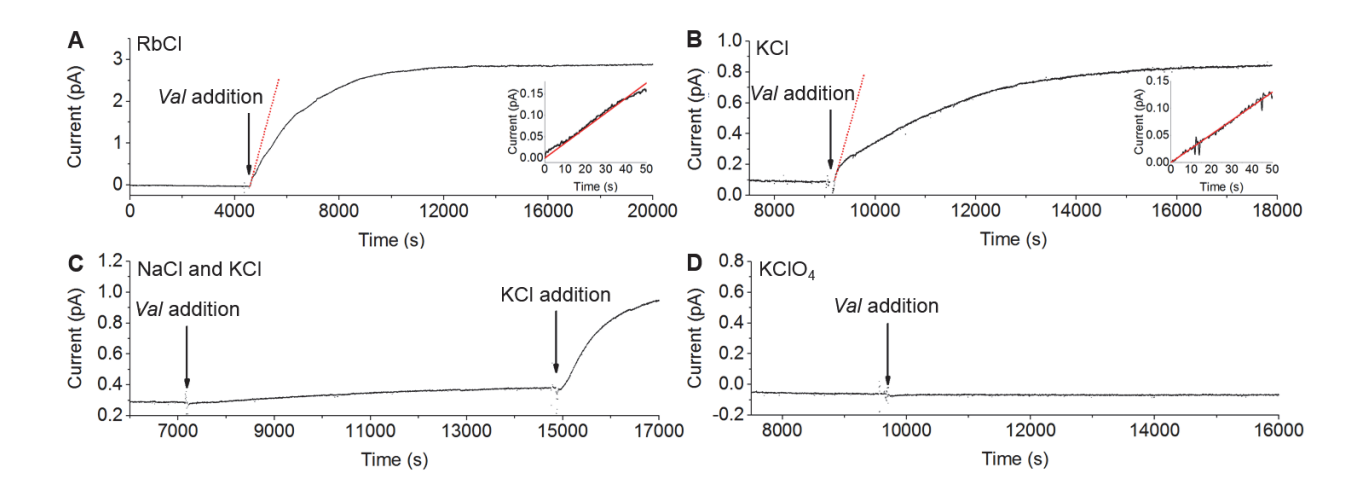


Figure 3. *i-t* traces of *val*-mediated ion transport in (A) 0.5 M RbCl, (B) 0.5 M KCl, (C) 0.5 M NaCl, and (D) 0.1 M KClO<sub>4</sub> solutions. Trials were initiated at t = 0 s in their respective electrolyte solutions containing 10 mM phosphate buffer (PB), pH 7.4 at  $V_{app} = 0.1$  V. After a baseline current was measured, the external solution was exchanged with the same electrolyte solution containing, in addition,  $1.5 \times 10^{-6}$  M val (A, B, D) or  $5.0 \times 10^{-7}$  M val (C) (indicated by "Val addition"). The red line (—) in (A) and (B) and insets show the numerical fits of eq (3) ( $vide\ infra$ ), which describes the rate of val insertion into the membrane, to the first 50 seconds of the i-t trace following val addition. Following the addition of val in trace (C), 100  $\mu$ L of the NaCl/val solution was removed from the bulk solution at  $\sim 15,000$  s and replaced by 100  $\mu$ L of 0.5 M KCl (indicated by "KCl addition"). In (D), no significant current increase is observed in the KClO<sub>4</sub> solution after addition of val. Nanopore radii = 358 nm (A–C) and 468 nm (D).

The steady-state current obtained ~2 hr after the introduction of *val* results from the depletion of *val* in the bulk solution, a consequence of its adsorption onto the polycarbonate (PC) surface comprising the experimental cell (See experiments presented in the Supporting Information detailing *val* adsorption onto PC, Figures S4–S5, and Table S3). The adsorption onto

the PC surface is irreversible on the timescale of our experiments and occurs in parallel with val entering the bilayer, resulting in the concentration of val in the 300  $\mu$ L PC cell decreasing to negligible values within ~2 hr. After reaching  $i_{ss}$ , the electrical current remains constant over the course of the experiment (measured up to ~8 hr), including experiments in which the existing val solution is replaced by the buffer electrolyte solution (Figure S6). These results suggest that val is irreversibly adsorbed into the membrane lipid phase and torus region. As shown below, the adsorption of val onto PC surfaces is an important advantage in our investigations, limiting the number of val that are active in transporting cations.

Figure 3C demonstrates the enhanced ion selectivity of val for K<sup>+</sup> over Na<sup>+</sup>, as expected based on the ~ $10^5$  greater binding constant of val to K<sup>+</sup> relative to Na<sup>+</sup>. $^{44, 46-48}$  A bilayer baseline current was first obtained in 0.5 M NaCl, followed by introduction of val into the bulk solution. Val spontaneously inserts into the membrane transporting Na<sup>+</sup>, as indicated by the establishment of  $i_{ss} \approx 100$  fA, relative to bilayer baseline. A 100  $\mu$ L aliquot of the 0.5 M NaCl/val solution was removed from the experimental cell and replaced with a 100  $\mu$ L aliquot of 0.5 M KCl. The current increased immediately upon the introduction of K<sup>+</sup>, approaching a new  $i_{ss}$  value of ~800 fA. We attribute this increase to the higher binding efficiency of val to K<sup>+</sup> at the electrolyte/bilayer interface (step (i) in Figure 1) relative to Na<sup>+</sup>.

Previous literature has reported that when *val* is dissolved in the lipid phase *prior* to membrane formation, the *val*(K<sup>+</sup>) transport current is larger in the presence of ClO<sub>4</sub><sup>-</sup> relative to Cl<sup>-</sup>. <sup>32, 33, 49</sup> We reproduced the current enhancement of *val*(K<sup>+</sup>) in the presence of ClO<sub>4</sub><sup>-</sup> when *val* is pre-dissolved in the lipid phase (Figures S7–S9). The results of Figure 3D, however, suggest that the presence of ClO<sub>4</sub><sup>-</sup> in the bulk electrolyte solution prevents the spontaneous insertion of *val* 

from the bulk solution into the bilayer. We speculate ClO<sub>4</sub><sup>-</sup> may block *val* from inserting into the bilayer due to ClO<sub>4</sub><sup>-</sup> affiliating with the zwitterionic DPhPC phospholipid head-groups.<sup>50-52</sup>

The Electrical Current Associated with Individual *Val* Ionophores. Having established that our nanopore system yields *val*-mediated transport behavior in agreement with prior reports, we next addressed the possibility of measuring the electrical current associated with an individual *val* ionophore. Based on the estimated current associated with one *val* transporting K<sup>+</sup> ( $\Delta i \approx 1.5$  fA), the number of *val* associated with  $i_{ss}$  can be estimated as  $N_v = i_{ss}/1.5$  fA. For example, from the data obtained in 0.5 M KCl solution containing  $1.5 \times 10^{-6}$  M *val*, Figure 3B,  $i_{ss} \approx 700$  fA and  $N_v \approx 470$  *val*. This value of  $N_v$  suggests the possibility of measuring changes in the current,  $\Delta i$ , associated with a single *val* resulting from small statistical fluctuations in  $N_v$ . We find that  $i_{ss}$ , and thus  $N_v$ , can be further reduced by an order of magnitude by decreasing the initial concentration of *val* in the electrolyte solution. Figure 4A shows a i-t trace recorded in 0.5 M KCl before and after introducing  $2.0 \times 10^{-8}$  M *val*, resulting in an current increase that reaches  $i_{ss} = 40$  fA (as measured from the baseline) after  $\sim 2,500$  s, corresponding to  $\sim 30$  *val* in the membrane. Figure 4B shows an i-t trace recorded in the same conditions as Figure 4A, but in the absence of *val*.

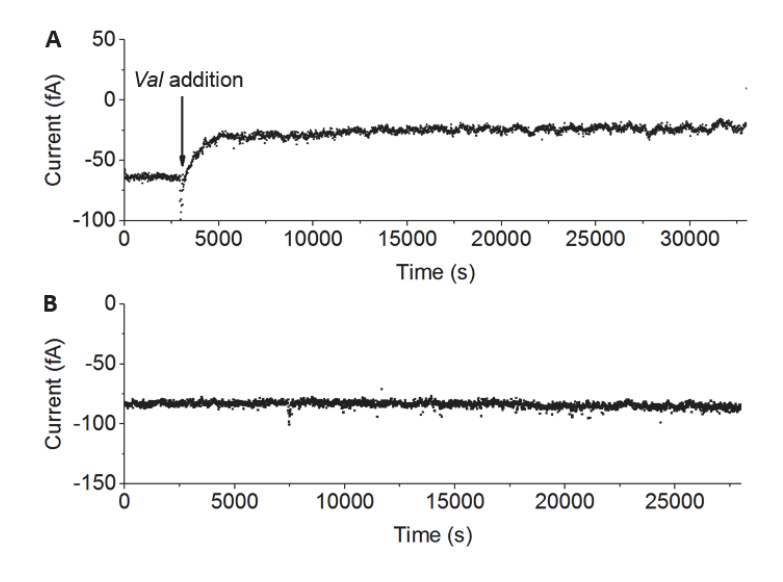


Figure 4.  $Val(K^+)$  transport v.s. bilayer baseline. (A) i-t trace of  $val(K^+)$  transport using  $2.0 \times 10^{-8}$  M val. (B) i-t trace of a lipid bilayer without val. Trials each began in 0.5 M KCl and 10 mM PB, pH 7.4 at  $V_{app}$ = 0.1 V. After the baseline measurement was stable in (A), a complete solution exchange was performed to introduce val by replacing the original electrolyte solution with the same electrolyte solution containing  $2.0 \times 10^{-8}$  M val. Nanopore radii = 358 nm (A) and 468 nm (B).

Exchange of val between the bilayer and torus region, as initially proposed by Stark and coworkers to explain their observed dependence of val facilitated current on the radius of the bilayer, is expected to lead to small time-dependent fluctuations in the number of active val in the bilaver. 14 Ideally, when a single val enters or leaves the membrane, there is a corresponding step increase or decrease in the current due to a change in the small number of ionophores. Inspection of an expanded 400 s region of the *i-t* trace, Figure 5A, indeed shows step-like features that are partially obscured by electronic noise. However, similar features are not observed in *i-t* traces prior to the addition of val, Figure 5C, or in additional control experiments where val is absent, which indicates the current steps result from val mediated ion transport and not experimental noise. A step identification program (SIP) was written (see Supporting Information, Figures S10, S16, and Table S4) to identify current steps in the *i-t* traces and quantify the magnitude of the step change,  $\Delta i$ , resulting from val partitioning between the bilayer and torus region. Briefly, the steps are identified based on the slope,  $\pm M_{\text{range}}$  (pA/s), of N data points to distinguish between regions of constant current from regions when the current changes due to a val entering or leaving the bilayer. Regions of the data with similar current averages are grouped together based on a tolerance range, T(%).

The *i-t* traces generated by the SIP are shown in Figure 5A and 5C, overlaid on the experimental data. Figure 5B and 5D are histograms of  $\Delta i$  values, corresponding to the full 7.8

hour-long *i-t* traces recorded in the presence and absence of *val* shown in Figure 4. The bimodal histogram in Figure 5B corresponds to *val* partitioning between the membrane and torus region, with the two peaks centered at  $\Delta i = \pm 1.3 \pm 0.6$  fA. The bimodal and symmetric distribution of  $\pm \Delta i$  is expected, since  $i_{ss}$  is constant. SIP analysis of an independent experiment yields  $\Delta i = \pm 1.2 \pm 0.5$  fA (Figure S13).

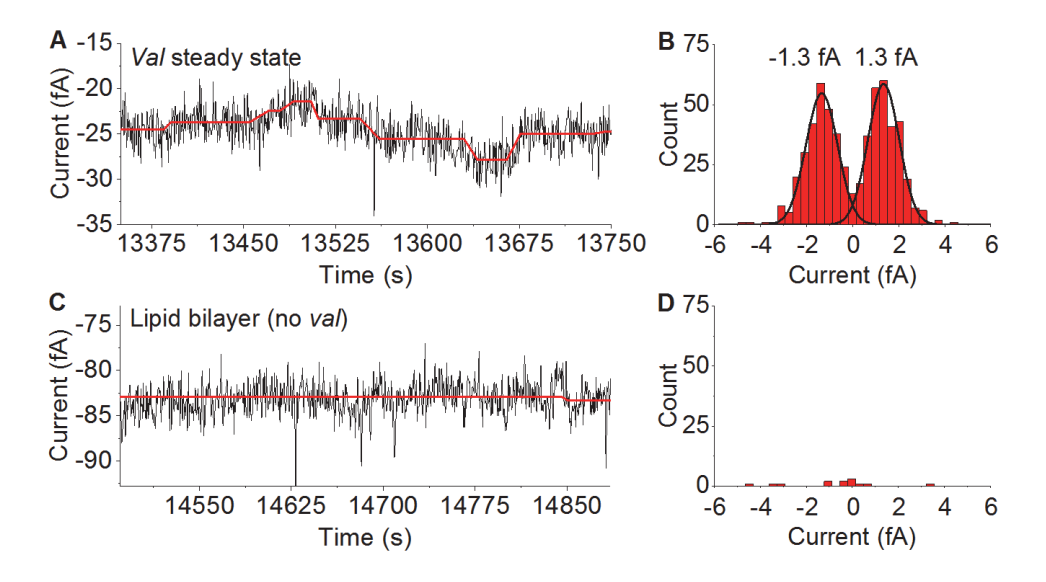


Figure 5. The SIP analysis of the current response in the presence ((A) and (B)) and absence ((C) and (D)) of *val*. The *val*  $i_{ss}$  corresponds to an average of ~30 *val* molecules present in the membrane. (A) and (C) show a representative 400 s section of the *i-t* traces from Figure 4. The red line (—) corresponds to the SIP analysis trace (additional examples shown in Figures S11–S12). The analysis was completed on 7.8 hours of data shown in Figure 4A (5,000–33,000 s) and 4B (0–28,000 s). Histogram (B) corresponds to 583 events where  $\Delta i = \pm 1.3 \pm 0.6$  fA identified by the SIP. SIP parameters are: N = 10,  $M_{range} = \pm 1.8 \times 10^{-4}$  pA/s, T = 4.16%.

We estimate that *val* partition events occur every ~50 s, (Figure S14), which is comparable to an estimate from the bandwidth of a power spectral density of the current noise in the presence of *val* (Figure S15). During the 50 s lifetime of a *val* molecule in the bilayer, it would be responsible

for passing an average electrical charge of ~410,000  $e^-$ . As previously discussed, shot noise represents a fundamental limit that defines the minimum current required to quantify an event. However, all electrical measurements have an additional non-zero background current, which contributes to the shot noise. From Figure 5A, the 1.3 fA current steps are measured on a background current of ~25 fA, yielding a theoretical limit of quantification of 3,900  $e^-$  / $\Delta t$  (see Supporting Information). The measured electrical charge of ~410,000  $e^-$  observed during the measurement time,  $\Delta t = 50$  s, is thus ~100× larger than the minimum required to accurately quantify the current associated with one val.

To assess the accuracy of the SIP analysis, we created a simulated i-t trace comprising idealized current steps of  $\Delta i = \pm 1.3$  fA (Figure 6). These simulated steps were added to an experimental i-t trace of a bilayer baseline (no val) acquired at 5 kHz with a 1 kHz LPF (Figure 6A-B). The sum of the experimental baseline and simulated current steps were then resampled at 2 Hz with a 1 Hz LPF (Figure 6C). The SIP analysis was applied to this synthetic data to assess how well it identified current steps and quantified values of  $\Delta i$ . We found that the SIP successfully identified all simulated current steps, (Figure 6D), and yielded  $\Delta i$  values (1.3 ±0.2 fA) in agreement with expected values (1.3 fA). Thus, the larger variation observed in the experimental  $\Delta i$  values  $(1.3 \pm 0.6 \text{ fA})$  likely reflects real differences in the current carried by individual val. The slow SIP transition times of  $\sim 20$  s between val partition events are artifacts of the SIP analysis, as is evident by differences in the slope between the transitions in the SIP traces shown in Figure 6D-F. To further assess the SIP accuracy, two different regions of the experimental bilayer baseline were added to the idealized  $\pm 1.3$  fA current steps, and re-analyzed as before to yield  $\Delta i_{(E)} = 1.2 \pm 0.1$  fA and  $\Delta i_{\rm (F)} = 1.2 \pm 0.1$  fA (Figure 6E–F). Additionally, the effect of data sampling frequency was considered by comparing  $\Delta i$  values obtained from SIP analysis of simulated data sampled at 2 Hz (Figure 6D) and at 10 Hz (Figure 6G). No significant effect of the sampling rate on step identification or  $\Delta i$  was observed (Figure 6H). The SIP analysis of the experimental i-t traces were also found to be independent of sampling rate (Figure S12). These assessments indicate that the SIP is reliable in quantifying experimental  $\Delta i$  values.

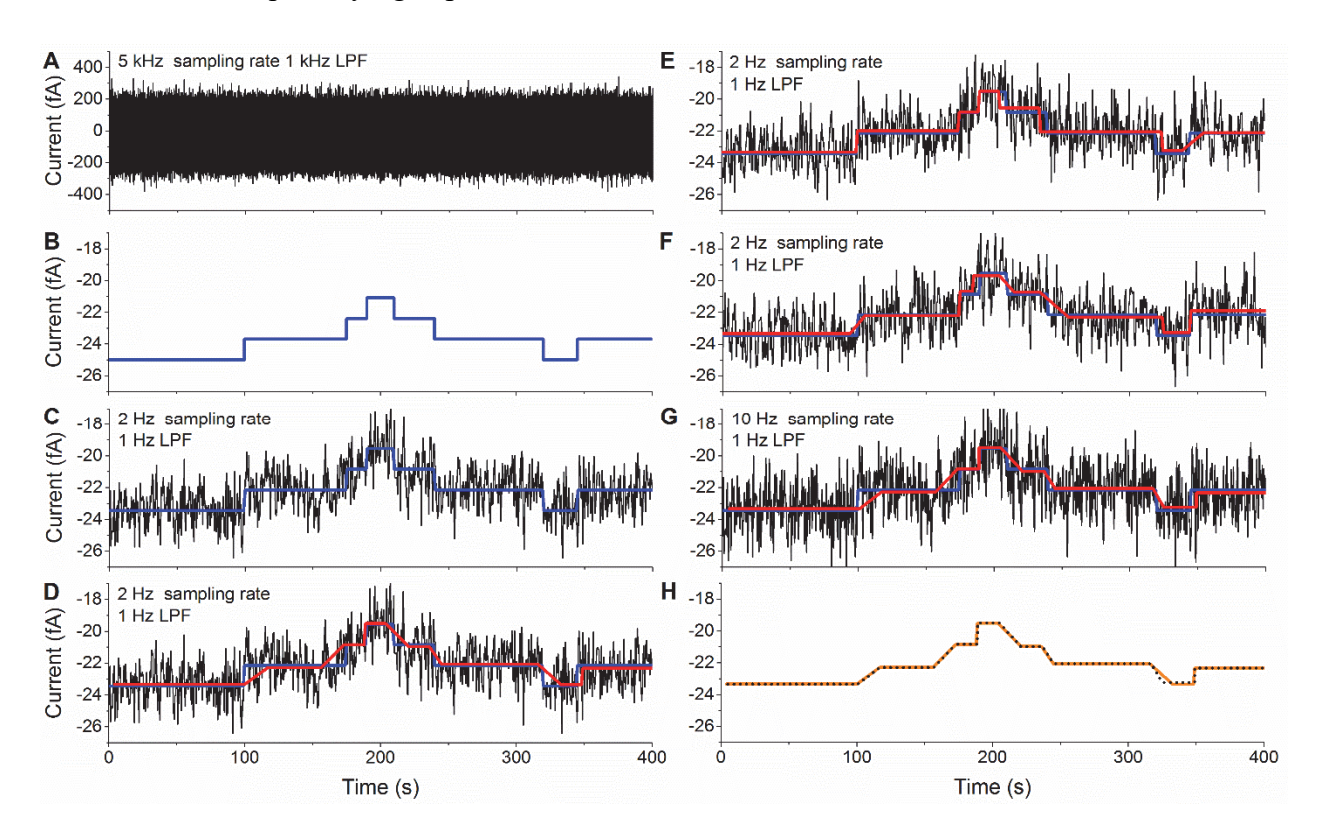


Figure 6. Assessment of the SIP using a simulated data set comprising ideal  $\pm 1.3$  fA steps. (A) Experimentally obtained i-t trace of a bilayer sampled at 5 kHz with a 1 kHz LPF. (B) Simulated  $\pm 1.3$  fA current steps (—). (C) The sum of the baseline current (from (A)) and simulated current steps (from (B)) and resampled at 2 Hz with a 1 Hz LPF. (D) Simulated data (from (C)) analyzed with the SIP to yield the red trace (—) with  $\Delta i_{(D)} = 1.3 \pm 0.2$  fA. The simulated i-t trace with added 1.3 fA current steps (—) is plotted in (C) and the SIP-identified current steps (—) are compared in (D). (E and F) An identical analysis was performed using different sections of the experimental i-t trace, yielding  $\Delta i_{(E)} = 1.2 \pm 0.1$  fA and  $\Delta i_{(F)} = 1.2 \pm 0.1$  fA. (G) The same simulated data shown in (C) but sampled at 10 Hz. (H) Comparison of the SIP

analysis from (D) at a 2 Hz sampling rate (—) with (G) at a 10 Hz sampling rate (···). SIP parameters are:  $N_{\text{(D-F)}} = 10$  and  $N_{\text{(G)}} = 50$ ,  $M_{\text{range}} = \pm 1.8 \times 10^{-4} \text{ pA/s}$ , T = 4.16%.

Kinetics of *Val* Insertion into the Bilayer Membrane. Measurement of  $\Delta i$  allows the rate constant of *val* entering the bilayer membrane from the electrolyte,  $k_{\rm f}$ , to be estimated from the *i*-t responses shown in Figure 3. At short times, the rate of insertion (val/s) is given by:

$$R = C_{v}AN_{A}k_{f}t \tag{2}$$

where  $C_v$  is the concentration of val in the bulk supporting electrolyte, A is the area of the bilayer,  $N_A$  is Avogadro's number, and  $k_f$  is the rate of val insertion into the membrane. Since each molecule contributes a current of  $\Delta i \approx 1.3$  fA to the observed current, the i-t trace at short times is described by:

$$i(t) = \Delta i C_{\rm v} A N_{\rm A} k_{\rm f} t \tag{3}$$

All parameters in eq (3) except  $k_f$  are previously measured ( $\Delta i C_v A$ ) or a constant ( $N_A$ ). Values of  $k_f$  were estimated by fitting eq (3) to the first 50 s of the experimental i-t traces after the addition of val, with this assumption that  $C_v$  does not change significantly due to adsorption on the PC cell walls during this initial time. We measured  $k_f$  to be between  $5.6 \times 10^{-9}$  and  $8.7 \times 10^{-8}$  cm/s for K<sup>+</sup> insertion based on 10 trials in 0.5 M KCl (Figure 3, Figure S3, and Table S2), and  $1.9 \times 10^{-8}$  for Rb<sup>+</sup> insertion based on one trial (Figure 3, Figure S3, Table S2).

## CONCLUSIONS

In conclusion, we have directly measured the electrical current associated with an individual val ionophore transporting  $K^+$  across a suspended lipid bilayer. The current associated with an individual ionophore,  $\Delta i$ , is the fundamental descriptor of ionophore transport efficiency

and is thus important in understanding the activity of ionophores when employed as antibiotic or antiviral agents. Each molecule of val was found to be responsible for  $1.3 \pm 0.6$  fA of K<sup>+</sup> transport at  $V_{app} = 0.1$  V, which, theoretically, is  $\sim 100 \times$  larger that the smallest current that can be quantified, assuming that the electrical noise arises from the discrete nature of electric charge. Such sensitive electrical methods using nanopore methods should be readily extended to other carrier-type ionophores of interest.

## **METHODS**

Chemicals and Materials. All chemicals were purchased from Sigma-Aldrich and used as received unless otherwise specified. Val was purchased as a lyophilized powder from Focus Biomolecules (Plymouth Meeting, PA) and suspended in MeOH and stored at -20°C. MeOH was evaporated and val was re-suspended in 16.5 µL of 200 proof EtOH. The val-EtOH solution was then diluted with 4.98 mL of the electrolyte solution to achieve a 0.33% EtOH solution by volume. EtOH is necessary to improve val solubility in aqueous solutions. The addition of EtOH to the system did not impact bilayer stability (Figure S2). All solutions were prepared using H2O purified with a Thermo Scientific Barnstead Smart2Pure water system (resistivity  $\geq 18 \text{ M}\Omega$  cm). Electrolyte solutions containing 0.5 M KCl, 0.5 M NaCl, 0.5 M RbCl, or 0.1 M KClO<sub>4</sub> buffered with 10 mM phosphate buffer, pH 7.2, were filtered using a sterile 0.22 µm Millipore filter. The phospholipid 1,2-diphytanoyl-sn-glycero-3-phosphocholine (DPhPC) was obtained from Avanti Polar Lipids (Alabaster, AL) and diluted with decane to a concentration of 10 mg/mL. Quartz nanopore supports were obtained from Electronic BioSciences (Salt Lake City, Utah). Nanopores were chemically modified with 2% (v/v) 3-cyanopropyldimetyhlchlorosilane in dry acetonitrile. 35, <sup>39</sup> A nanopore radius between 200-500 nm is ideal for this application as the small surface area of the formed membranes limits the number of inserted *val*, but are large enough to where the lipid leaflets can be joined with external pressure.

**Ion Transport Recordings.** The current-time (i-t) measurements were performed using a low noise Nanopatch system (Electronic BioSciences, Salt Lake City, Utah). The current was sampled at 5 kHz and filtered using an 8-pole Bessel low-pass filter at 1 kHz. Lipid bilayers were formed by gently adding a 0.05 µL aliquot of the lipid solution to the surface of the bulk supporting electrolyte, followed by raising and lowering the solution level with respect to the stationary nanopore to deposit two lipid leaflets across the nanopore opening.<sup>35, 39</sup> Once the lipid was deposited across the nanopore, the two lipid leaflets were joined by applying and maintaining a pressure of 20 mmHg from the interior of the nanopore using a gas-tight syringe.<sup>35, 39, 41</sup> A 0.1 V bias was applied across two Ag/AgCl electrodes on either side of the lipid bilayer to drive the valmediated ion transport from the bulk solution into the interior of the glass nanopore membrane. The resistance of the formed bilayers was recorded to assess its stability. Only membranes with a resistance of  $\sim 1 \text{ T}\Omega$  were used in the presented studies, indicating minimal leakage current through the bilayer. To introduce val to the experimental cell, complete solution exchanges were performed by replacing the original electrolyte solution with the electrolyte/val solution. The flow-cell design of the experimental cell allowed us to flow 1 mL of the new solution through the 300 µL experimental cell, effectively replacing all of the original electrolyte solution. The temperature was controlled by a custom PID thermoelectric cooler (CUI Inc., CP20151) and a thermocouple residing in the external reservoir. All experiments were performed at 23°C.

**Data Analysis.** Post data collection, the i-t traces were filtered using a 3-pole Butterworth low-pass filter at 1 Hz and resampled at 2 Hz. A step identification program (SIP) was used to quantify

 $\Delta i$ . The current steps are identified in the step analysis based on the slope,  $\pm M_{range}$  (pA/s), of N number of data points to determine where the current is constant and when it is changing due to a val partition event. Regions of the data with similar current averages are grouped together based on a tolerance range,  $\pm T$  (%). A complete description of the SIP can be found in Figures S10, S16, and at the end of this SI in the 'Step Identification Program Source Code' section. The variability in the reported  $\Delta i$  value is the standard deviation of the measurement.

### **AUTHOR INFORMATION**

#### **Corresponding Authors**

Joel M. Harris – Department of Chemistry, University of Utah, Salt Lake City, Utah 84112, United States; https://orcid.org/0000-0002-7081-8188

Henry S. White – Department of Chemistry, University of Utah, Salt Lake City, Utah 84112, United States; https://orcid.org/0000-0002-5053-0996

#### **Authors**

Alexandra J. Schmeltzer – Department of Chemistry, University of Utah, Salt Lake City, Utah 84112, United States; https://orcid.org/0000-0003-1873-2413

#### **Conflict of Interests**

H.S.W. is a co-inventor on patent number US 8,581,605 B2 governed by the University of Utah Research Foundation that covers the fabrication and use of glass nanopores.

## **ACKNOWLEDGEMENTS**

This work was supported by the Office of Naval Research (N00014-22-1-2425) and the National Science Foundation (CHE-1904424).

#### SUPPORTING INFORMATION AVAILABLE

Calculations of *val* rate constants within lipid bilayers; studies assessing lipid bilayer stability; additional examples of *val* membrane insertion kinetics; studies of *val* adsorption onto polycarbonate materials; lifetimes of *val* in the lipid bilayer; studies detailing *val* pre-dissolved in the lipid phase prior to membrane formation; step identification program (SIP) description and source code; additional examples of the SIP analysis; evaluation of the frequency of *val* partition events; and calculations of the shot noise limit of quantification in the presence of a baseline.

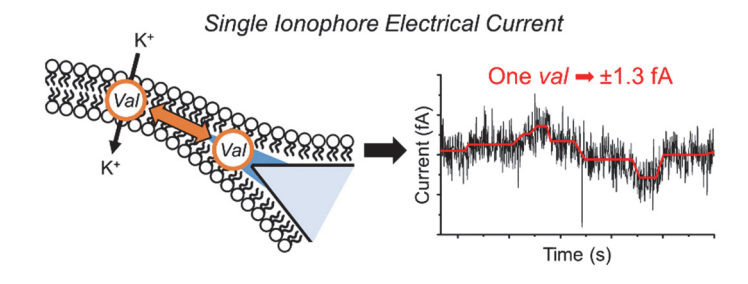
## REFERENCES AND NOTES

- 1. Moore, C.; Pressman, B. C. Mechanism of Action of Valinomycin on Mitochondria. *Biochem. Biophys. Res. Commun.* **1964**, *16*, 562-567.
- 2. Pressman, B. C. Induced Active Transport of Ions in Mitochondria. *Proc. Natl. Acad. Sci. U. S. A.* **1965**, *53*, 1076-1083.
- 3. Reed, P. W. Ionophores. *Methods Enzymol.* **1979**, *55*, 435-454.
- 4. Frahm, D. H. In Vitro Studies on the Antibacterial Action of Valinomycin. Ph.D. Thesis, Creighton University, Omaha Nebraska, USA, 1971.
- 5. Wibowo, J. T.; Kellermann, M. Y.; Kock, M.; Putra, M. Y.; Murniasih, T.; Mohr, K. I.; Wink, J.; Praditya, D. F.; Steinmann, E.; Schupp, P. J. Anti-Infective and Antiviral Activity of Valinomycin and Its Analogues from a Sea Cucumber-Associated Bacterium, Streptomyces sp. SV 21. *Marine drugs* **2021**, *19*, 81.
- 6. Zhang, D.; Ma, Z.; Chen, H. C.; Lu, Y. L.; Chen, X. L. Valinomycin As a Potential Antiviral Agent Against Coronaviruses: A Review. *Biomed J* **2020**, *43*, 414-423.
- 7. Brockmann, H.; Schmidtkastner, G. Valinomycin I, XXVII. Mitteil. über Antibiotica aus Actinomyceten. *Chem. Ber. Recl.* **1955**, *88*, 57-61.
- 8. Brockmann, H.; Geeren, H. Valinomycin II. Antibiotika Aus Actinomyceten XXXVII. Die Konstitution Des Valinomycins. *Annalen Der Chemie-Justus Liebig* **1957**, *603*, 216-232.
- 9. Baltscheffsky, H.; Arwidsson, B. Evidence for two phosphorylation sites in bacterial cyclic photophosphorylation. *Biochim. Biophys. Acta* **1962**, *65*, 425-428.
- 10. Wang, C. Y.; Polovitskaya, M. M.; Delgado, B. D.; Jentsch, T. J.; Long, S. B. Gating Choreography and Mechanism of the Human Proton-activated Chloride Channel ASOR. *Sci Adv* **2022**, *8*, p.eabm3942.
- 11. He, W. Y.; Wang, C. Y.; Wang, H. M.; Jian, M. Q.; Lu, W. D.; Liang, X. P.; Zhang, X.; Yang, F. C.; Zhang, Y. Y. Integrated Textile Sensor Patch for Real-time and Multiplex Sweat Analysis. *Sci Adv* **2019**, *5*, p.eaax0649.
- 12. Wu, C. Y.; Jan, J. T.; Ma, S. H.; Kuo, C. J.; Juan, H. F.; Cheng, Y. S. E.; Hsu, H. H.; Huang, H. C.; Wu, D.; Brik, A.; Liang, F. S.; Liu, R. S.; Fang, J. M.; Chen, S. T.; Liang,

- P. H.; Wong, C. H. Small Molecules Targeting Severe Acute Respiratory Syndrome Human Coronavirus. *Proc. Natl. Acad. Sci. U. S. A.* **2004**, *101*, 10012-10017.
- 13. Altendorf, K.; Epstein, W.; Lohmann, A. Valinomycin-Induced Cation-Transport in Vesicles Does Not Reflect the Activity of K+-Transport Systems in Escherichia-Coli. *J. Bacteriol.* **1986**, *166*, 334-337.
- 14. Benz, R.; Stark, G.; Janko, K.; Lauger, P. Valinomycin-Mediated Ion-Transport through Neutral Lipid-Membranes Influence of Hydrocarbon Chain-Length and Temperature. *J. Membr. Biol.* **1973**, *14*, 339-364.
- 15. Carrasquel-Ursulaez, W.; Reeves, R. D.; Dehghany, M.; Jones, C.; Schomaker, J. M.; Chanda, B. Re-Evaluation of the Mechanism of Cytotoxicity of Dialkylated Lariat Ether Compounds. *Rsc Adv* **2020**, *10*, 40391-40394.
- 16. Cranfield, C. G.; Bettler, T.; Cornell, B. Nanoscale Ion Sequestration To Determine the Polarity Selectivity of Ion Conductance in Carriers and Channels. *Langmuir* **2015**, *31*, 292-298.
- 17. David, J. M.; Rajasekaran, A. K. Gramicidin A: A New Mission for an Old Antibiotic. *Journal of kidney cancer and VHL* **2015**, *2*, 15-24.
- 18. Freedman, J. C. Ionophores in Planar Lipid Bilayers. In *Cell Physiology Source Book: Essentials of Membrane Biophysics*, 4th ed.; Sperelakis, N.; Elsevier Academic Press, San Diego, **2012**; pp. 61-66.
- 19. Ghadiri, M. R.; Granja, J. R.; Buehler, L. K. Artificial Transmembrane Ion Channels from Self-Assembling Peptide Nanotubes. *Nature* **1994**, *369*, 301-304.
- 20. Halsey, C. M.; Benham, D. A.; Jiji, R. D.; Cooley, J. W. Influence of the Lipid Environment on Valinomycin Structure and Cation Complex Formation. *Spectrochim Acta A* **2012**, *96*, 200-206.
- 21. Howe, E. N. W.; Busschaert, N.; Wu, X.; Berry, S. N.; Ho, J. M.; Light, M. E.; Czech, D. D.; Klein, H. A.; Kitchen, J. A.; Gale, P. A. pH-Regulated Nonelectrogenic Anion Transport by Phenylthiosemicarbazones. *J. Am. Chem. Soc.* **2016**, *138*, 8301-8308.
- 22. Lauger, P. Kinetic-Properties of Ion Carriers and Channels. *J. Membr. Biol.* **1980**, *57*, 163-178.
- 23. Lauger, P.; Stark, G. Kinetics of Carrier-Mediated Ion Transport across Lipid Bilayer Membranes. *Biochim. Biophys. Acta* **1970**, *211*, 458-466.
- 24. Lee, M. T.; Yang, P. Y.; Charron, N. E.; Hsieh, M. H.; Chang, Y. Y.; Huang, H. W. Comparison of the Effects of Daptomycin on Bacterial and Model Membranes. *Biochemistry-Us* **2018**, *57*, 5629-5639.
- 25. Leevy, W. M.; Weber, M. E.; Gokel, M. R.; Hughes-Strange, G. B.; Daranciang, D. D.; Ferdani, R.; Gokel, G. W. Correlation of Bilayer Membrane Cation Transport and Biological Activity in Alkyl-Substituted Lariat Ethers. *Org Biomol Chem* **2005**, *3*, 1647-1652.
- 26. Podrazka, M.; Maciejewska, J.; Adamiak, W.; Nery, E. W.; Jonsson-Niedziolka, M. Facilitated Cation Transfer at a Three-Phase Junction and its Applicability for Ionophore Evaluation. *Electrochim. Acta* **2019**, *307*, 326-333.
- 27. Pressman, B. C. Biological Applications of Ionophores. *Annu. Rev. Biochem* **1976**, *45*, 501-530.
- 28. Prindle, A.; Liu, J. T.; Asally, M.; Ly, S.; Garcia-Ojalvo, J.; Suel, G. M. Ion Channels Enable Electrical Communication in Bacterial Communities. *Nature* **2015**, *527*, 59-63.

- 29. Ross, E. E.; Hoag, B.; Joslin, I.; Johnston, T. Measurements of Ion Binding to Lipid-Hosted Ionophores by Affinity Chromatography. *Langmuir* **2019**, *35*, 9410-9421.
- 30. Stark, G.; Ketterer, B.; Benz, R.; Lauger, P. The Rate Constants of Valinomycin-mediated Ion Transport Through Thin Lipid Membranes. *Biophys. J.* **1971**, *11*, 981-994.
- 31. Wu, X.; Judd, L. W.; Howe, E. N. W.; Withecombe, A. M.; Soto-Cerrato, V.; Li, H.; Busschaert, N.; Valkenier, H.; Perez-Tomas, R.; Sheppard, D. N.; Jiang, Y. B.; Davis, A. P.; Gale, P. A. Nonprotonophoric Electrogenic Cl- Transport Mediated by Valinomycin-like Carriers. *Chem-Us* **2016**, *1*, 127-146.
- 32. Shirai, O.; Yoshida, Y.; Kihara, S. Voltammetric Study on Ion Transport Across a Bilayer Lipid Membrane in the Presence of a Hydrophobic Ion or an Ionophore. *Anal Bioanal Chem* **2006**, *386*, 494-505.
- 33. Onishi, J.; Shirai, O.; Kano, K. Electrochemical Elucidation of the Facilitated Ion Transport Across a Bilayer Lipid Membrane in the Presence of Neutral Carrier Compounds. *Electroanal* **2010**, *22*, 1229-1238.
- 34. Edelwejn, Z.; Jeljasze.J; Szmigiel.S; Zak, C. Brain Bioelectric Activity in Staphylococcal Alpha-Hemolysin Intoxication. *Toxicol. Appl. Pharmacol.* **1968**, *13*, 133-145.
- 35. White, R. J.; Ervin, E. N.; Yang, T.; Chen, X.; Daniel, S.; Cremer, P. S.; White, H. S. Single Ion-channel Recordings Using Glass Nanopore Membranes. *J. Am. Chem. Soc.* **2007**, *129*, 11766-11775.
- 36. Kelkar, D. A.; Chattopadhyay, A. The Gramicidin Ion Channel: a Model Membrane Protein. *Biochim. Biophys. Acta* **2007**, *1768*, 2011-2025.
- 37. Stark, G.; Benz, R. The Transport of Potassium Through Lipid Bilayer Membranes by the Neutral Carriers Valinomycin and Monactin: Experimental Studies to a Previously Proposed Model. *J. Membr. Biol.* **1971**, *5*, 133-153.
- 38. Gao, R.; Edwards, M. A.; Harris, J. M.; White, H. S. Shot Noise Sets the Limit of Quantification in Electrochemical Measurements. *Curr Opin Electroche* **2020**, *22*, 170-177.
- 39. Zhang, B.; Galusha, J.; Shiozawa, P. G.; Wang, G. L.; Bergren, A. J.; Jones, R. M.; White, R. J.; Ervin, E. N.; Cauley, C. C.; White, H. S. Bench-top Method for Fabricating Glass-sealed Nanodisk Electrodes, Glass Nanopore Electrodes, and Glass Nanopore Membranes of Controlled Size. *Anal. Chem.* **2007**, *79*, 4778-4787.
- 40. White, S. H. Analysis of the Torus Surrounding Planar Lipid Bilayer Membranes. *Biophys. J.* **1972**, *12*, 432-445.
- 41. Schibel, A. E. P.; Heider, E. C.; Harris, J. M.; White, H. S. Fluorescence Microscopy of the Pressure-Dependent Structure of Lipid Bilayers Suspended across Conical Nanopores. *J. Am. Chem. Soc.* **2011**, *133*, 7810-7815.
- 42. Mueller, P.; Rudin, D. O. Development of K+ Na+ Discrimination in Experimental Bimolecular Lipid Membranes by Macrocyclic Antibiotics. *Biochem. Biophys. Res. Commun.* **1967**, *26*, 398-404.
- 43. Markin, V. S.; Krishtalik, L. I.; Liberman, Y. A.; Topaly, V. P. Mechanism of Conductivity of Artificial Phospholipid Membranes in Presence of Ion Carriers. *Biophys-Ussr* **1969**, *14*, 272-282.
- 44. Varma, S.; Sabo, D.; Rempe, S. B. K+/Na+ Selectivity in K Channels and Valinomycin: Over-coordination Versus Cavity-size Constraints. *J. Mol. Biol.* **2008**, *376*, 13-22.

- 45. Liesegang, G. W.; Eyring, E. M. Kinetic Studies of Synthetic Multidentate Macrocyclic Compounds. In *Synthetic Multidentate Macrocyclic Compounds*, 1st ed.; Izatt, R. M., Christensen, J. J.; Academic Press, New York, **1978**; pp. 283-308.
- 46. Grell, E.; Funck, T.; Eggers, F. Structure and Dynamic Properties of Ion-specific Antibiotics. *Membranes* **1975**, *3*, 1-126.
- 47. Minami, H.; Sato, N.; Sugawara, M.; Umezawa, Y. Comparative-Study on the Potentiometric Responses between a Valinomycin-Based Bilayer Lipid-Membrane and a Solvent Polymeric Membrane. *Anal. Sci.* **1991**, *7*, 853-862.
- 48. Stepanova, S.; Kasicka, V. Affinity Capillary Electrophoresis Applied to Investigation of Valinomycin Complexes with Ammonium and Alkali Metal Ions. *Methods in molecular biology* **2016**, *1466*, 219-232.
- 49. Su, Z.; Ran, X.; Leitch, J. J.; Schwan, A. L.; Faragher, R.; Lipkowski, J. How Valinomycin Ionophores Enter and Transport K(+) across Model Lipid Bilayer Membranes. *Langmuir* **2019**, *35*, 16935-16943.
- 50. Li, X. Z., J.; Xie X. The Hofmeister Anion Effect on Ionophore-based Ion-selective Nanospheres Containing Solvatochromic Dyes. *Electroanal* **2020**, *32*, 749-754.
- 51. Pokorna, S.; Jurkiewicz, P.; Cwiklik, L.; Vazdar, M.; Hof, M. Interactions of Monovalent Salts with Cationic Lipid Bilayers. *Faraday Discuss.* **2013**, *160*, 341-358.
- 52. Wu, X.; Wang, P.; Lewis, W.; Jiang, Y. B.; Gale, P. A. Measuring anion binding at biomembrane interfaces. *Nat Commun* **2022**, *13*, 1-7.



For Table of Contents Only